processes

MDPI

Article

An Equivalent Fracture Element-Based Semi-Analytical Approach to Evaluate Water-Flooding Recovery Efficiency in Fractured Carbonate Reservoirs

Wenqi Zhao [1], Lun Zhao [1,*], Qianhui Wu [1,*], Qingying Hou [1], Pin Jia [2] and Jue Hou [1]

[1] PetroChina Research Institute of Petroleum Exploration & Development, China National Petroleum Corporation, Beijing 100083, China; zhaowenqi@petrochina.com.cn (W.Z.); houqingying@petrochina.com.cn (Q.H.); houjue95@petrochina.com.cn (J.H.)
[2] School of Petroleum Engineering, China University of Petroleum, Beijing 102249, China; jiapin@cup.edu.cn
* Correspondence: zhaolun@petrochina.com.cn (L.Z.); wuqh0803@163.com (Q.W.)

Abstract: The productivity prediction of weakly volatile fractured reservoirs is influenced by reservoir parameters and fluid characteristics. To address the computational challenges posed by complex fractures, an equivalent fracture element method is proposed to calculate equivalent permeability in fractured zones. A three-phase seepage model based on material balance is developed, using the Baker linear model to determine the relative permeabilities of oil, gas, and water while accounting for bound water saturation. Dynamic drainage distance and conductivity coefficients are introduced to calculate production at each stage, with the semi-analytical model solved iteratively for pressure and saturation. Validation against commercial simulation software confirms the model's accuracy, enabling the construction of productivity curves and analysis of reservoir characteristics and injection scenarios. Results showed that the equivalent fracture element method effectively handled multiphase nonlinear seepage and predicted productivity during water flooding. Productivity was more sensitive to through-fracture models, with production increasing as the fracture extent expanded. Optimal water injection occurred when the formation pressure dropped to 80% of the bubble point pressure, and the recovery efficiency improved with periodic-injection strategies compared to conventional methods. These findings have significant implications for improving oil recovery, optimizing injection strategies, and advancing the design of efficient reservoir management techniques across scientific, practical, and technological domains.

Keywords: weakly volatile fractured reservoir; water flooding; equivalent fracture element; dynamic drainage area; recovery

check for updates

Academic Editor: Qingbang Meng

Received: 9 October 2024
Revised: 25 November 2024
Accepted: 3 December 2024
Published: 3 January 2025

Citation: Zhao, W.; Zhao, L.; Wu, Q.; Hou, Q.; Jia, P.; Hou, J. An Equivalent Fracture Element-Based Semi-Analytical Approach to Evaluate Water-Flooding Recovery Efficiency in Fractured Carbonate Reservoirs. *Processes* **2025**, *13*, 96. https://doi.org/10.3390/pr13010096

Copyright: © 2025 by the authors. Licensee MDPI, Basel, Switzerland. This article is an open access article distributed under the terms and conditions of the Creative Commons Attribution (CC BY) license (https://creativecommons.org/licenses/by/4.0/).

1. Introduction

Naturally fractured reservoirs play an important role in the oil and gas industry framework [1]. These fractures intersect with each other to form a fracture network, serving as a conduit for groundwater flow within the rock masses [2]. The flow through fractured rock is affected by the geometry of the fracture network [3]. The occurrence, location, size, and distribution of fractures are not uniform, complicating the study of fracture characteristics [4]. Two primary methods for analyzing seepage in fractured reservoirs are the discontinuous method and the equivalent continuum method [5]. To facilitate calculations, various equivalent models are used in different fractured reservoirs [6]. Because fractures are not completely connected in the reservoir, fracture connectivity and boundary

conditions have a great influence on the determination of equivalent permeability, which leads to large errors in these methods [7]. Snow [8] employed the parallel plate theory to represent the actual properties of fracture distribution. Long [9] studied the influence of the connectivity degree among fractures on the equivalent permeability. Sagar [10] derived the equivalent Darcy permeability equation, and the fracture state examined did not completely penetrate the reservoir.

The current methods for predicting productivity in fractured reservoirs mostly consist of analytical, semi-analytical, and numerical simulation techniques. The analytical approach involves formulating the productivity calculation equation for a fractured reservoir predicated on steady-state flow conditions. Liu [11] computed the horizontal well productivity for both infinite formation and boundary formation utilizing analytical formulas. Ji [12] proposed a novel analytical model for complicated fractured horizontal wells, incorporating non-Darcy seepage and stress sensitivity. Sureshjani et al. [13] developed a novel analytical model that accounts for the non-volume effects of marginal aquifers in the production data analysis of single-phase reservoirs. Wang [14] enhanced the traditional trilinear flow model, formulated the mathematical model for single-phase fracturing fluid flowback, and derived the analytical solution for bottomhole pressure during this process via the Laplace transform method. A weakly volatile fractured reservoir entails multiphase unsteady seepage and presents significant nonlinear challenges.

The analytical method is limited to calculating productivity. The semi-analytical method essentially entails analyzing and deriving the problem to obtain an analytical formulation, then employing numerical calculation techniques for the solution. Chen [15] developed a semi-analytical model for horizontal wells in rectangular closed reservoirs with discrete fracture networks under variable internal boundary conditions. Wang [16] established a horizontal well seepage mathematical model based on the dual porosity model considering imbibition and adopted a semi-analytical multi-well production prediction method to solve it. Currently, the semi-analytical productivity prediction of fractured reservoirs is mainly focused on oil–water two-phase flow, and the semi-analytical method of oil–water multiphase seepage has yet to be studied. At present, the numerical simulation methods for fractured reservoirs mainly use finite-volume methods and other numerical methods to construct fracture grids [17–20], simulate reservoir development, and evaluate productivity. This method needs to encrypt the fracture grid, resulting in a large number of grids and a slow calculation speed. To sum up, the difficulties in productivity prediction for fractured reservoirs are as follows: first, it is difficult to deal with fracture networks, and second, the accuracy of oil and gas two-phase flow and production capacity prediction is low.

Based on the analysis of cores with different fracture occurrences, this paper puts forward the equivalent fracture element method and uses the fracture equivalent transformation to build a three-phase oil–gas–water seepage mathematical model. The dynamic oil drainage distance (DDA) proposed by Qanbari and Clarkson [21] is introduced, and the material balance method and Newton iterative solution are used to form a set of water-driven oil–gas semi-analytical methods. Moreover, the influencing factors are analyzed. Compared with the experimental method, the numerical simulation results show that the method has less error, higher calculation efficiency and accuracy, and lays a theoretical foundation for the productivity prediction of fractured reservoirs.

2. Materials and Methods

2.1. Materials

Fracture reservoirs are highly heterogeneous. Figure 1 depicts the actual fractured core in the field, whereas Figure 2 illustrates the schematic diagram of the fractured reservoir.

The fracture distribution and permeability calculation in the fracture area of the model are complex, and the reservoir exhibits significant heterogeneity.

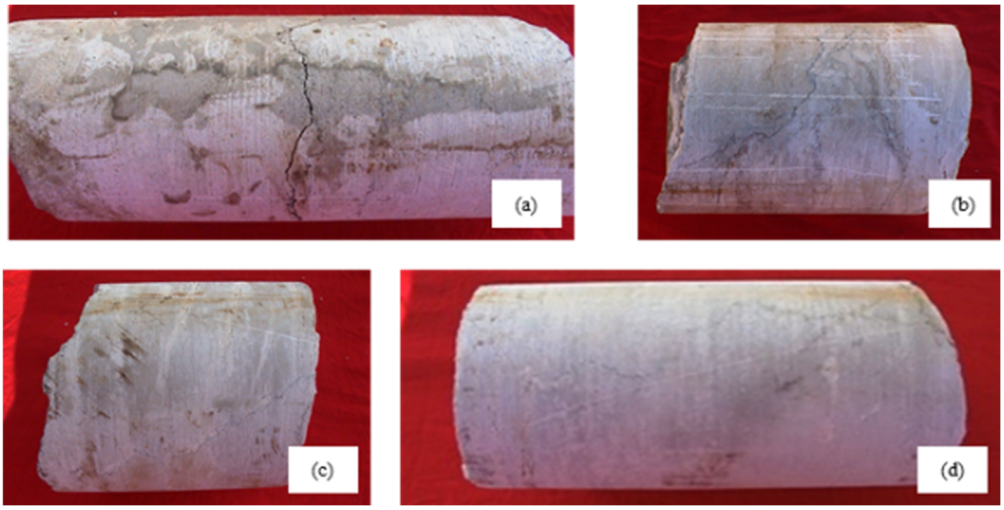


Figure 1. Actual core on-site. Core samples depicted in (**a**–**d**) are from different locations.

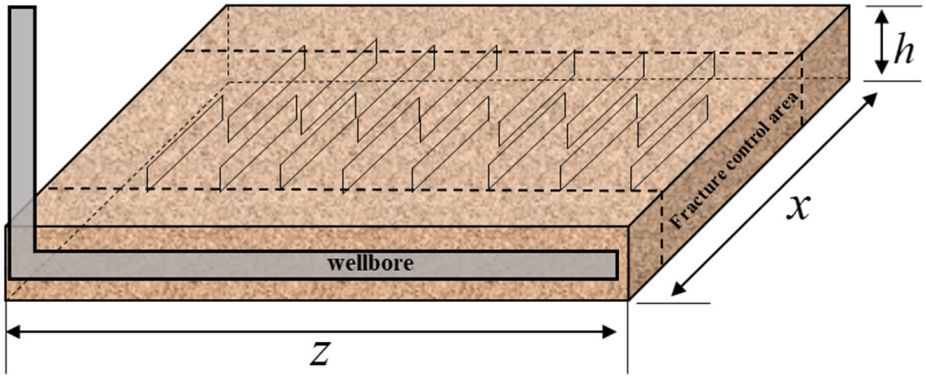


Figure 2. Schematic of the fractured reservoir.

2.2. Methods

The fracture development points of cores with different fracture occurrences were analyzed, and the common fracture units of four types of fracture occurrences were extracted, as shown in Figure 3. At present, there is little research on the semi-analytical productivity calculation method of fractured reservoirs. At the same time, the existence of fractures greatly influences the calculation of production, which increases the difficulty of calculating oil and gas production using the semi-analytical method. Therefore, a concept using the equivalent fracture element method is proposed in this paper. According to Darcy's law, under the same pressure difference and fluid properties of a homogeneous core, this paper obtained the same flow rate by changing the permeability.

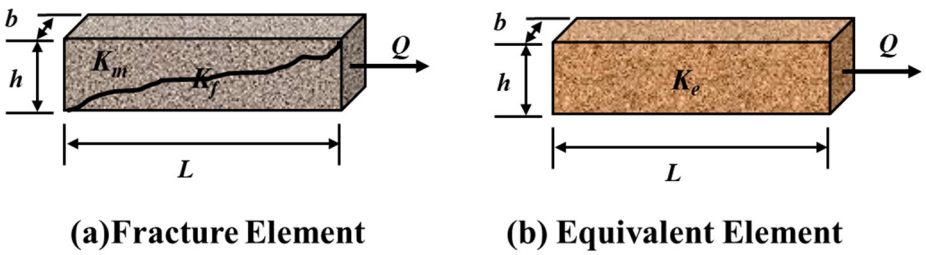


Figure 3. Comparison of physical models of a fractured core and homogeneous core.

As shown in Figure 3b, the homogeneous equivalent model has the same parameters as the fracture unit except for permeability, and this physical unit is called the equivalent fracture element in this paper.

The calculation of equivalent permeability is described in Equation (1) below [22]:

$$K_f = \frac{\phi_f b^2}{12} \tag{1}$$

where b is the fracture element width, cm, ϕ_f is the fracture porosity, %, and K_f is the fracture permeability, cm^2.

The fracture model in Figure 4 consists of the matrix and fracture body. The total flow rate, Q (cm^3/s), through the model is equal to the sum of flow rate through the matrix (Q_m) and flow rate through the fracture (Q_f) [23–26]. The flow rate through the matrix can be expressed as Equation (2):

$$Q_m = \frac{K_m b_m h}{\mu} \frac{\Delta p}{l} \tag{2}$$

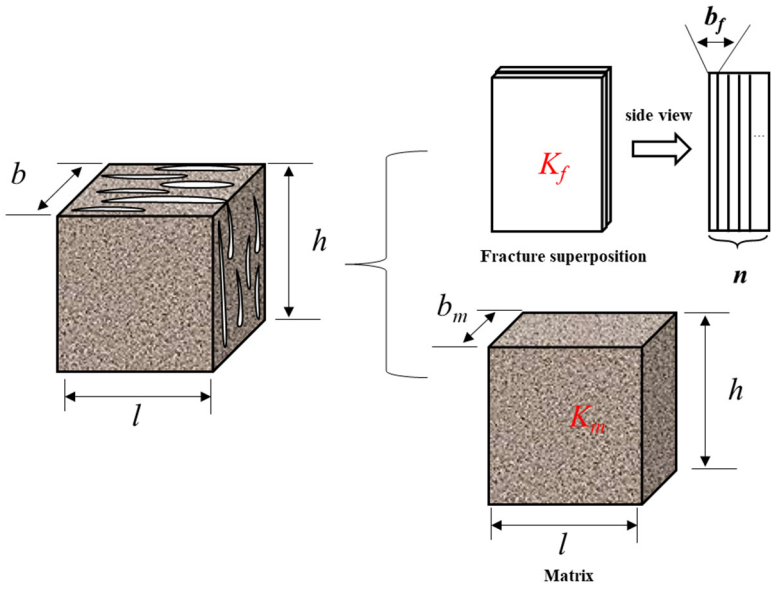


Figure 4. Comparison of physical models of a fractured core and homogeneous core.

The flow rate through the fracture can be calculated by Equation (3):

$$Q_f = \frac{K_f b_f b D_f h}{\mu} \frac{\Delta p}{l} \tag{3}$$

where K_m and K_f are matrix and fracture permeability, D; b is the total width of the fracture model, cm; bm is the width of the pure matrix, cm; b_f is the fracture opening, cm; D_f is the fracture linear density, n/b; l is the length of the model, cm; h is the height of the model, cm; μ is the viscosity of the injection fluid, cP; Δp is the pressure drop, atm. Suppose there is an equivalent permeability K_e (Equation (4)), such that:

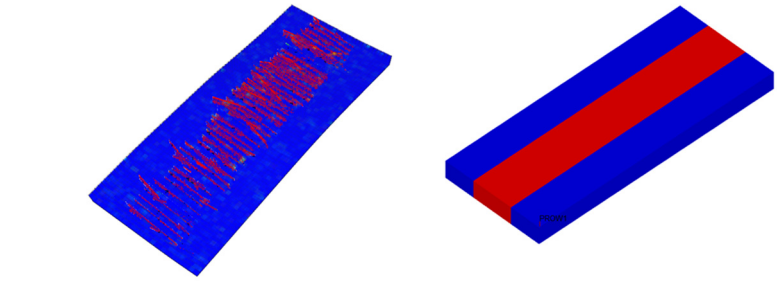
$$Q = \frac{K_e b h}{\mu} \frac{\Delta p}{l} = Q_m + Q_f \tag{4}$$

Introducing Q_f and Q_m into the above formula, the equivalent permeability can be obtained simultaneously, as illustrated in Equation (5):

$$K_e = K_m + \left(K_f - K_m\right) D_f b_f \tag{5}$$

2.3. Verification by Equivalent Fracture Element Method

The numerical model of the fractured reservoir and the corresponding equivalent change model were constructed (Figure 5). The matrix permeability was 30 mD, the fracture opening was 0.1 mm, and the fracture linear density was 5 fractures/m. The equivalent permeability was calculated according to the fracture distribution range, and the corresponding numerical model was also constructed.



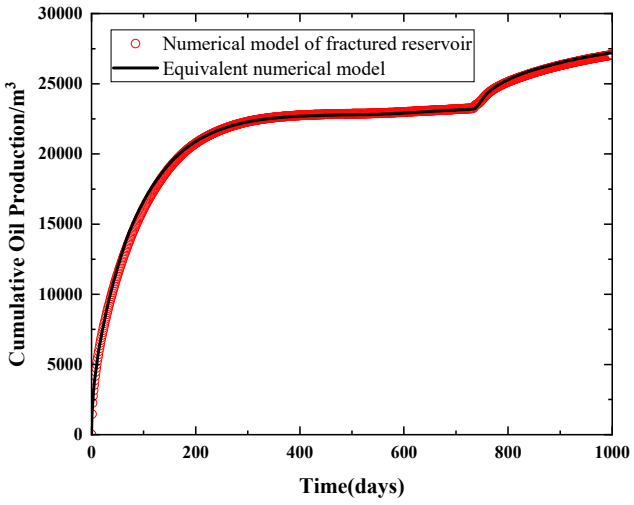
(a) Numerical model of fractured reservoir (b) Equivalent numerical model

Figure 5. Fracture numerical model and numerical model after equivalent transformation. Red indicates the fractured zones, while blue denotes the matrix.

Table 1 lists the simulation parameters for the mechanistic model, simulating the case of fixed bottom-hole flow pressure for 500 days of depletion followed by 500 days of water injection. Figure 6 compares the oil and gas production between the two methods.

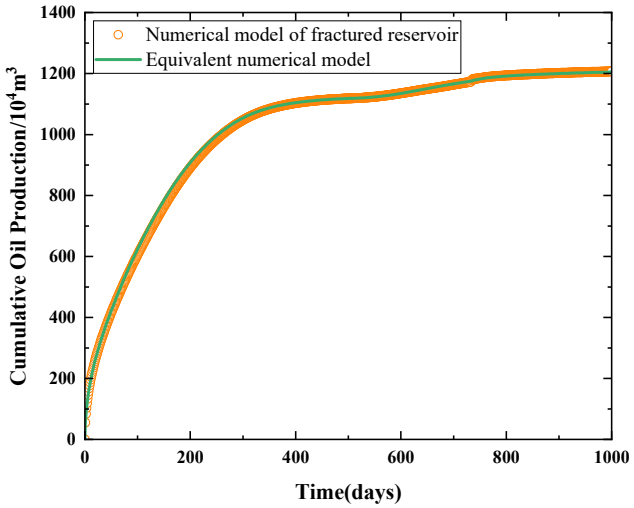
Table 1. Model parameter settings.

Model Parameters	Values
Initial pressure (MPa)	24
Saturation pressure (MPa)	21
Size of grid (m)	40
Number of grids	100 × 1 × 25
Initial oil saturation (%)	72
Matrix permeability (mD)	30
Fracture permeability (mD)	500



(a)

Figure 6. *Cont.*



(**b**)

Figure 6. Oil and gas production comparison results. (**a**) Cumulative oil production comparison. (**b**) Cumulative gas production comparison.

As shown in Figures 7 and 8, the cumulative production of equivalent transformation models of different occurrences was compared, and the maximum error of cumulative production was less than 1%. The verification results showed that the method was highly accurate and in line with the engineering accuracy of the reservoir.

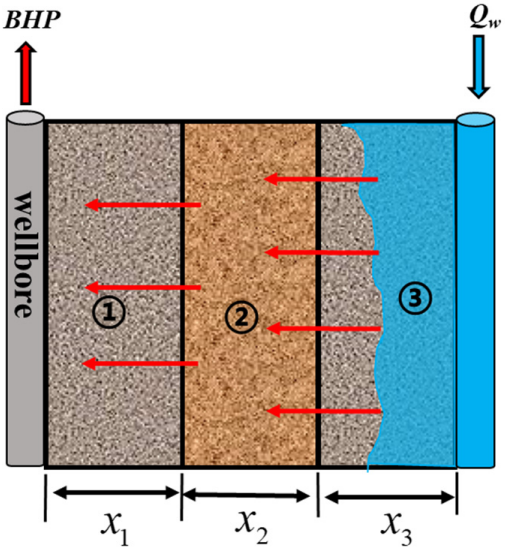


Figure 7. Physical model based on the equivalent fracture element.

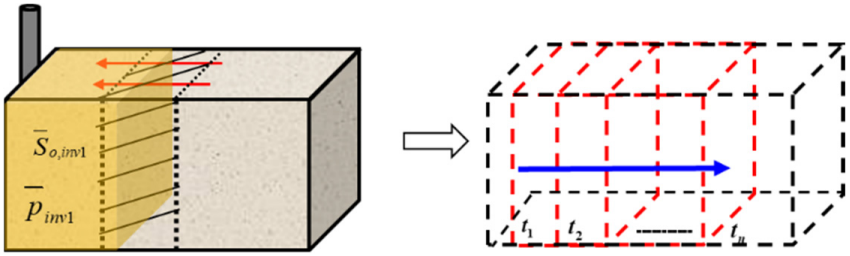


Figure 8. Dynamic drainage distance principle.

2.4. Physical Model Based on Equivalent Fracture Element

Figure 7 shows the three-zone heterogeneous physical model of a fractured reservoir based on equivalent transformation. The reservoir properties of the inner and outer areas were the same, and the permeability of the fracture area was calculated by the equivalent fracture unit method. The following assumptions were made [27,28]:

(1) The porosity and initial oil saturation of the zones are the same.
(2) The reservoir is equal in thickness, and the influence of gravity is ignored.
(3) The compressibility of fluids and rocks is considered.
(4) The fluid consists of three phases, i.e., oil, gas, and water, and the dissolved gas content in the oil phase is characterized by R_s, the solution gas–oil ratio, m^3/m^3.

3. Results and Discussions

3.1. Three-Zone, Three-Phase Mathematical Model

In this section, the equivalent permeability of the fracture zone was calculated after equivalent transformation according to the equivalent fracture unit. A mathematical model of three-zone oil and gas two-phase flow was constructed based on the principle of material balance and the consideration of bound water saturation.

3.1.1. Region Far from the Wellbore

The remote well area was the matrix area, so only the outflow of oil and gas was considered. Due to the outer defined flow rate injection, injection and inflow of water into the fracture area were considered simultaneously. In the early stage of the development of the volatile reservoir, there was a single-phase oil flow in the reservoir, and the two-phase oil and gas flow occurred when the local layer pressure dropped below the bubble point pressure. When the injection well was positioned at the boundary of the reservoir, the oil, gas, and water three-phase flow occurred. Therefore, considering the inflow of the water phase and the fluid supply to the fracture zone, the governing equation for the seepage flow in the remote well area can be obtained as follows (Equations (6)–(9)):

$$\begin{cases} \frac{\partial}{\partial x}\left[\frac{\beta k_3 k_{ro}}{\mu_o B_o}\frac{\partial p}{\partial x}\right] = \frac{\partial}{\partial t}\left(\frac{\phi S_o}{B_o}\right) \\ \frac{\partial}{\partial x}\left[\left(\frac{R_s \beta k_3 k_{ro}}{\mu_o B_o} + \frac{\beta k_3 k_{rg}}{\mu_g B_g}\right)\frac{\partial p}{\partial x}\right] = \frac{\partial}{\partial t}\left(\frac{R_s \phi S_o}{B_o} + \frac{\phi S_g}{B_g}\right) \\ \frac{\partial}{\partial x}\left[\frac{\beta k_3 k_{rw}}{\mu_w B_w}\frac{\partial p}{\partial x}\right] + q_w = \frac{\partial}{\partial t}\left(\frac{\phi S_w}{B_w}\right) \end{cases} \quad (6)$$

$$\text{Initial condition}: \ p_3|_{t=0} = p_i \quad (7)$$

We considered the external boundary conditions for a constant flow rate:

$$\left.\frac{\partial p_{3out}}{\partial x}\right|_{x=x3} = \frac{q}{\mu k_3 b h} \quad (8)$$

$$\text{Internal boundary condition}: \ q_{2flow-in} = q_{3flow-out} \quad (9)$$

where β is the unit conversion factor, which is 0.0864; k_3 represents the permeability of the area far from the wellbore, mD; k_{ro}, k_{rg}, and k_{rw} denote the relative permeabilities of the oil phase, gas phase, and water phase, respectively; μ_o, μ_g, and μ_w are the viscosity of oil, water, and gas, mPa·s; B_o, B_g, and B_w refer to the volume factors for the oil phase, gas phase, and water phase; S_o, S_g, and S_w represent the oil, gas, and water saturation; R_s signifies the solution gas–oil ratio, m^3/m^3; q_w pertains to the source term; $q_{2flow-in}$ denotes the inflow rate into the equivalent fracture zone from the region far from the wellbore, and $q_{3flow-out}$ indicates the outflow rate from this region to the equivalent fracture zone.

3.1.2. Equivalent Fracture Region

The fracture region was a double medium and a single homogeneous hyperpermeability region after equivalent transformation. In the prospective area, injected water flowed into the equivalent fracture area, and the original oil–gas two-phase seepage changed to oil–gas–water three-phase seepage in the equivalent fracture area, but the water phase had no source-sink term. In this case, the seepage control equation was as follows (Equations (10)–(13)):

$$\begin{cases} \frac{\partial}{\partial x}\left[\frac{\beta k_2 k_{ro}}{\mu_o B_o}\frac{\partial p}{\partial x}\right] = \frac{\partial}{\partial t}\left(\frac{\phi S_o}{B_o}\right) \\ \frac{\partial}{\partial x}\left[\left(\frac{R_s \beta k_2 k_{ro}}{\mu_o B_o} + \frac{\beta k_2 k_{rg}}{\mu_g B_g}\right)\frac{\partial p}{\partial x}\right] = \frac{\partial}{\partial t}\left(\frac{R_s \phi S_o}{B_o} + \frac{\phi S_g}{B_g}\right) \\ \frac{\partial}{\partial x}\left[\frac{\beta k_2 k_{rw}}{\mu_w B_w}\frac{\partial p}{\partial x}\right] = \frac{\partial}{\partial t}\left(\frac{\phi S_w}{B_w}\right) \end{cases} \tag{10}$$

$$\text{Initial condition}: \ p_2|_{t=0} = p_i \tag{11}$$

$$\text{Outer boundary condition}: q_{2flow-in} = q_{3flow-out} \tag{12}$$

$$\text{Internal boundary condition}: \ q_{1flow-in} = q_{2flow-out} \tag{13}$$

where K_2 is the equivalent permeability for the fractured region, and $q_{1flow\text{-}in}$ denotes the inflow rate into the equivalent fracture zone from the region far from the wellbore.

3.1.3. Near-Well Region

Similarly, in the near-well area, fluids flowing into the near-well area from the equivalent fracture area and into the wellbore from the near-well area need to be considered. In this case, the conservation equation was as follows (Equations (14)–(17)):

$$\begin{cases} \frac{\partial}{\partial x}\left[\frac{\beta k_1 k_{ro}}{\mu_o B_o}\frac{\partial p}{\partial x}\right] = \frac{\partial}{\partial t}\left(\frac{\phi S_o}{B_o}\right) \\ \frac{\partial}{\partial x}\left[\left(\frac{R_s \beta k_1 k_{ro}}{\mu_o B_o} + \frac{\beta k_1 k_{rg}}{\mu_g B_g}\right)\frac{\partial p}{\partial x}\right] = \frac{\partial}{\partial t}\left(\frac{R_s \phi S_o}{B_o} + \frac{\phi S_g}{B_g}\right) \\ \frac{\partial}{\partial x}\left[\frac{\beta k_1 k_{rw}}{\mu_w B_w}\frac{\partial p}{\partial x}\right] = \frac{\partial}{\partial t}\left(\frac{\phi S_w}{B_w}\right) \end{cases} \tag{14}$$

$$\text{Initial Conditions}: \ p_1|_{t=0} = p_i \tag{15}$$

$$\text{Outer boundary condition}: \ q_{1flow-in} = q_{2flow-out} \tag{16}$$

$$\text{Internal boundary condition}: \ q_{wflow-in} = q_{1flow-out} \tag{17}$$

where K_1 is the equivalent permeability of the fractured regions.

3.2. Semi-Analytical Solution of the Three-Phase Mathematical Model of Weakly Volatile Carbonate Rocks

3.2.1. Establishment of the Three-Phase Material Balance Equation

(1) Coupling of the far-well area, fracture area, and near-well area was performed using the material balance method. The cumulative production of each zone was equal to the difference between the initial geological reserves and the remaining geological reserves (Equation (18)) [21]:

$$\begin{cases} IOIP - ROIP = N_{pout,new} - N_{pin,new} \\ N_{p,new} = N_p + q_o \cdot \Delta t \end{cases} \tag{18}$$

where IOIP is the original geological reserves and *ROIP* is the existing geological reserves. $N_{p,out}$ is the cumulative output of each zone, $N_{p,in}$ is the cumulative inflow output of each zone, $N_{p,new}$ is the cumulative production under the current time step, N_p is the cumulative production under the previous time step, q is the instantaneous flow, and Δt is the unit time.

(2) The dynamic drainage radius was introduced to calculate the dynamic drainage area, and the dynamic drainage conductivity was calculated through the real-time dynamic drainage radius. When the pressure wave reached the boundary, the dynamic drainage distance was $x = \sqrt{6\eta_3 t}$, where η was calculated by Equation (19):

$$\eta = \frac{\rho_{wstd}\beta k_3 \frac{k_{rw3}}{\mu_{w3}B_{w3}} + \rho_{ostd}\beta k_3 \frac{k_{ro3}}{\mu_{o3}B_{o3}} + \rho_{gstd}\beta k_3 \left(\frac{R_s k_{ro3}}{\mu_{o3}B_{o3}} + \frac{k_{rg3}}{\mu_{g3}B_{g3}}\right)}{\rho_{wstd}\phi_3(c_3 + c_w)\frac{S_{w3}}{B_{w3}} + \rho_{ostd}\phi_3(c_3 + c_o)\frac{S_{o3}}{B_{o3}} + \rho_{gstd}\phi_3\left((c_3 + c_o)\frac{R_s S_{o3}}{B_{o3}} + (c_3 + c_g)\frac{S_{g3}}{B_{g3}}\right)} \quad (19)$$

When the pressure had spread to the boundary, the drainage distance was the length of the entire reservoir, i.e., $x = x_e$ [22]. Figure 8 illustrates the dynamic drainage process of oil recovery.

(3) The product of the dynamic conductivity coefficient and the difference between the original formation pressure and the pressure under the current time step proposed by Wattenbarger [23] was used (Equation (20)). Figure 9 schematically illustrates the variation of water saturation during water flooding.

$$\begin{cases} q = T_{cp}(p_i - p) \\ T_{cp} = \frac{kh}{1.842B\mu\left[\frac{2}{\pi}\left(\frac{x}{w}\right)\right]} \end{cases} \quad (20)$$

where q represents the instantaneous flow rate from zone m to zone n; T_{cp} denotes the dynamic conductivity coefficient; P_m is the average pressure in zone m, measured in MPa; P_n is the average pressure in zone n, also measured in MPa; km indicates the permeability of zone m, mD; B_j refers to the formation volume factor of fluid j; μ_j signifies the viscosity of fluid j, mPa·s; x represents the dynamic oil drainage distance, m; w denotes the width of the fracture zone, m; h is the thickness of the reservoir, m.

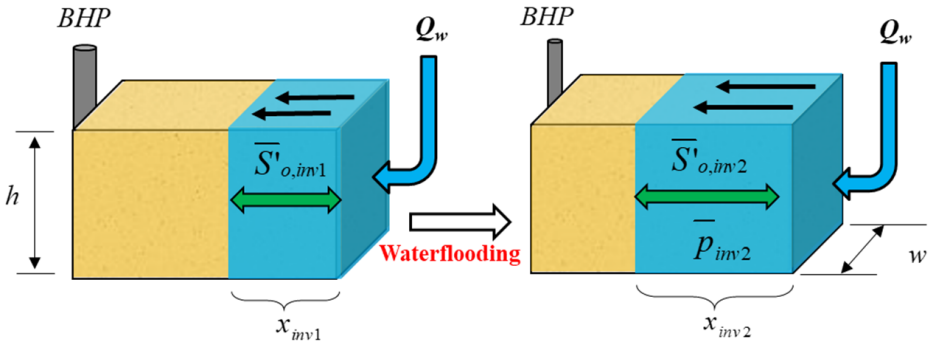


Figure 9. Schematic of the water saturation variation during water flooding.

(4) The simultaneous mass balance equations for each region were derived. At the beginning of water injection in the remote well area, the oil, water, and gas three-phase material balance equation in the three zones can be expressed as (Equation (21)):

$$\begin{cases} x_1zh\left(\frac{\phi_{1i}S_{o1i}}{B_{o1i}}-\frac{\phi_1\overline{S}_{o1}}{B_{o1}}\right)=\left[N_{ow1}+T_{ocp,w1}(\overline{p}_1-p_{w1})\Delta t\right]-\left[N_{o12}+T_{ocp,12}(\overline{p}_2-\overline{p}_1)\Delta t\right] \\ x_1zh\left(\frac{\phi_{1i}S_{g1i}}{B_{g1i}}-\frac{\phi_1\overline{S}_{g1}}{B_{g1}}\right)+x_1zh\left(\frac{R_{si}\phi_{1i}S_{o1i}}{B_{o1i}}-\frac{R_{s1}\phi_1\overline{S}_{o1}}{B_{o1}}\right)=\left[N_{gw1}+T_{gcp,w1}(\overline{p}_1-p_{w1})\Delta t\right] \\ -\left[N_{g12}+T_{gcp,12}(\overline{p}_2-\overline{p}_1)\Delta t\right]+\left[N_{ogw1}+T_{ogcp,w1}(\overline{p}_1-p_{w1})\Delta t\right]-\left[N_{og12}+T_{ogcp,12}(\overline{p}_2-\overline{p}_1)\Delta t\right] \\ x_1zh\left(\frac{\phi_{1i}S_{w1i}}{B_{w1i}}-\frac{\phi_1\overline{S}_{w1}}{B_{w1}}\right)=\left[N_{ww1}+T_{wcp,w1}(\overline{p}_1-p_{w1})\Delta t\right]-\left[N_{w12}+T_{wcp,12}(\overline{p}_2-\overline{p}_1)\Delta t\right] \\ x_2zh\left(\frac{\phi_{2i}S_{o2i}}{B_{o2i}}-\frac{\phi_2\overline{S}_{o2}}{B_{o2}}\right)=\left[N_{o21}+T_{ocp,21}(\overline{p}_2-\overline{p}_1)\Delta t\right]-\left[N_{o32}+T_{ocp,32}(\overline{p}_3-\overline{p}_2)\Delta t\right] \\ x_2zh\left(\frac{\phi_{2i}S_{g2i}}{B_{g2i}}-\frac{\phi_2\overline{S}_{g2}}{B_{g2}}\right)+x_2zh\left(\frac{R_{si}\phi_{2i}S_{g2i}}{B_{o2i}}-\frac{R_{s2}\phi_2\overline{S}_{g2}}{B_{o2}}\right)=\left[N_{g21}+T_{gcp,21}(\overline{p}_2-\overline{p}_1)\Delta t\right] \\ -\left[N_{g32}+T_{gcp,32}(\overline{p}_3-\overline{p}_2)\Delta t\right]+\left[N_{og21}+T_{ogcp,21}(\overline{p}_2-\overline{p}_1)\Delta t\right]-\left[N_{og32}+T_{ogcp,32}(\overline{p}_3-\overline{p}_2)\Delta t\right] \\ x_2zh\left(\frac{\phi_{2i}S_{w2i}}{B_{w2i}}-\frac{\phi_2\overline{S}_{w2}}{B_{w2}}\right)=\left[N_{w21}+T_{wcp,21}(\overline{p}_2-\overline{p}_1)\Delta t\right]-\left[N_{w32}+T_{wcp,32}(\overline{p}_3-\overline{p}_2)\Delta t\right] \\ x_3zh\left(\frac{\phi_{3i}S_{o3i}}{B_{o3i}}-\frac{\phi_3\overline{S}_{o3}}{B_{o3}}\right)=\left[N_{o32}+T_{ocp,32}(\overline{p}_3-\overline{p}_2)\Delta t\right] \\ x_3zh\left(\frac{\phi_{3i}S_{g3i}}{B_{g3i}}-\frac{\phi_3\overline{S}_{g3}}{B_{g3}}\right)+x_3zh\left(\frac{R_{si}\phi_{3i}S_{g3i}}{B_{g3i}}-\frac{R_{s3}\phi_3\overline{S}_{g3}}{B_{g3}}\right) \\ =\left[N_{g32}+T_{gcp,32}(\overline{p}_3-\overline{p}_2)\Delta t\right]+\left[N_{og32}+T_{ogcp,32}(\overline{p}_3-\overline{p}_2)\Delta t\right] \\ x_3zh\left(\frac{\phi_{3i}S_{w3i}}{B_{w3i}}-\frac{\phi_3\overline{S}_{w3}}{B_{w3}}\right)=\left[N_{w32}+T_{wcp,32}(\overline{p}_3-\overline{p}_2)\Delta t\right]+q_{winj}\Delta t \end{cases} \quad (21)$$

In Equation (21), x_j denotes the length of each sector, where j = 1, 2, 3, W represents the model width in meters, and h signifies the model thickness in meters. Φ_{ji} indicates the initial porosity of each region in percentage, and $\overline{S}_{lj}$ refers to the fluid saturation at the current time step for each region. The symbol B_{ij} represents the fluid formation volume factor under current pressure conditions for each region. The terms N_{lw1}, N_{l21}, and N_{l32} correspond to cumulative production from near-wellbore to wellbore, equivalent fracture zone to near-wellbore, and remote zone to equivalent fracture zone at the previous time step, respectively.$\overline{p_j}$ is the average pressure of each region at the current time step, P_{w1} denotes the wellbore pressure in MPa, q_{winj} represents injection terms, and Δt is time, measured in days.

3.2.2. Semi-Analytical Solution Process

The initial oil saturation of the model was 0.72, and the connate water saturation was 0.28, where the water phase did not flow, and the water saturation in this case was the connate water saturation. When the model pressure was lower than the saturation pressure, oil and gas two-phase seepage occurred. After water injection, water saturation and pressure increased in the remote well area, and the water phase began to flow. The sum of the three-phase saturation ($S_g + S_o + S_g$) was 1. The initial conditions for each sector are listed in Equation (22):

$$\begin{cases} P_1|_{t=0}=P_2|_{t=0}=P_3|_{t=0}=24MPa \\ S_{wc2}=S_{wc2}=S_{wc3}=0.28 \\ S_{oi1}=S_{oi2}=S_{oi3}=0.72 \end{cases} \quad (22)$$

The mean saturation and pressure at each time step in the three regions were calculated through the mass balance method to correct the nonlinear parameters in the semi-analytical model. By calculating the conductivity of each time step, the dynamic drainage distance was obtained to update the dynamic conductivity. Finally, the oil, gas, and water production in each region was obtained. The workflow for the calculation is summarized in Figure 10.

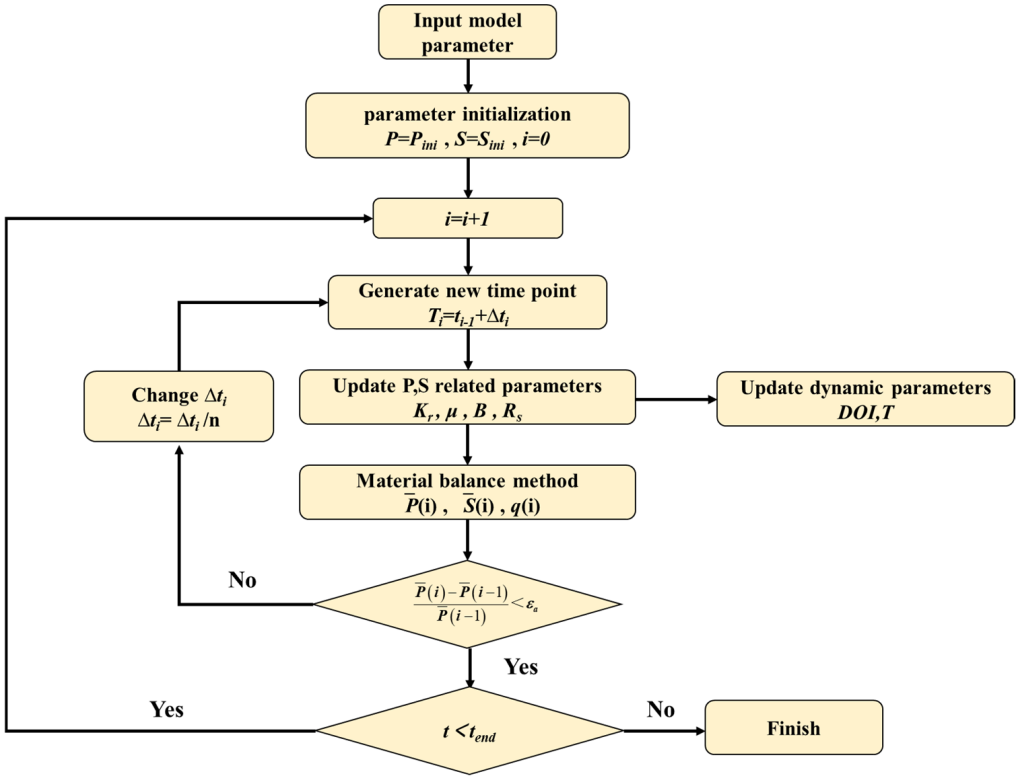


Figure 10. Workflow for solving the semi-analytical model.

3.2.3. Semi-Analytical Solution Method

In order to verify the accuracy of the established three-zone, three-phase semi-analytical model, the numerical model of the fractured reservoir after equivalent transformation was constructed and verified by tNavigator 23.1 numerical simulation software. The production well and injection well were both set with constant pressure and flow in the numerical model. The saturation of connate water was considered in the model. Only the connate water and oil were contained at the start of the model, and the dissolved gas precipitated after the pressure was reduced [28–30]. The water injection was performed after 365 days of depletion. Table 2 displays the specific model parameters, and Figure 11 displays the numerical model that was created following equivalent transformation.

Table 2. Model key parameters.

Parameters	Values
Near-wellbore permeability, mD	30
Equivalent permeability in fracture zone, mD	150
Remote well permeability, mD	30
Initial reservoir pressure, MPa	24
Length of near-well area, m	200
Fracture zone length, m	100
Length of remote well area, m	400
Formation compression factor, m	6.386×10^{-5}
Saturation pressure, MPa	21
Porosity, %	15

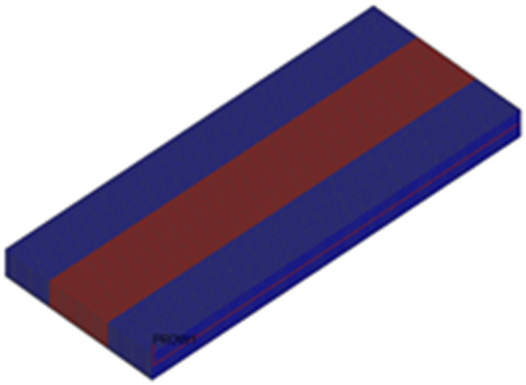


Figure 11. Numerical model. Red indicates the fractured zones, while blue denotes the matrix.

The fluid property parameters of this model were calculated by interpolating actual parameters of a fractured reservoir, as illustrated in Figure 12.

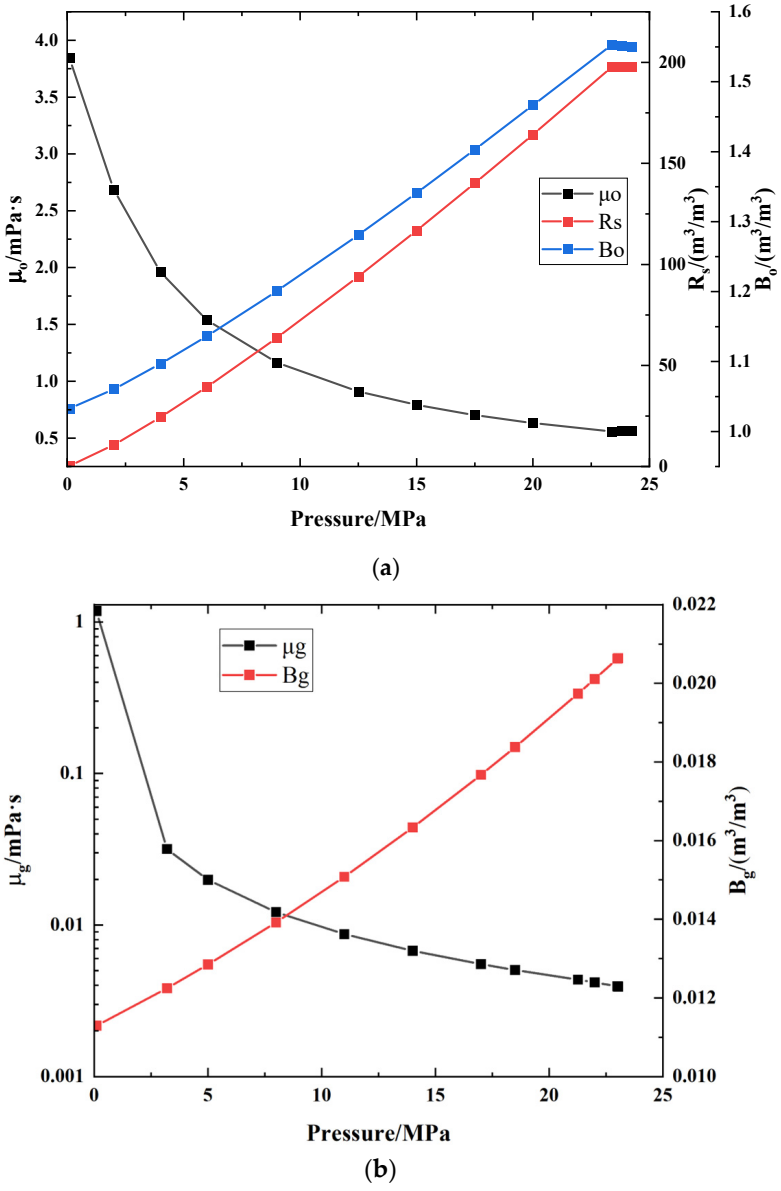


Figure 12. Fluid high-pressure physical property parameters: (**a**) oil PVT property and (**b**) gas PVT property.

Since this equivalent model equates the fracture region to the hyperpermeability matrix region, different relative permeability curves were adopted between the equivalent fracture region and the matrix, as shown in Figure 13. The Baker linear model was used in the semi-analytical model to calculate the relative permeability of oil, gas, and water (Equation (23)) [31]:

$$\begin{cases} k_{rO}(S_W, S_G) = \frac{S_G k_{rOG}(S_W+S_G-S_{Wc})+S_W k_{rOW}(S_W+S_G)}{S_G+S_W} \\ k_{rG}(S_W, S_G) = \frac{S_O k_{rGO}(S_G)+S_W k_{rGW}(S_G)}{S_O+S_W} \\ k_{rW}(S_W, S_G) = \frac{S_O k_{rWO}(S_W)+S_G k_{rWG}(S_W)}{S_O+S_G} \end{cases} \quad (23)$$

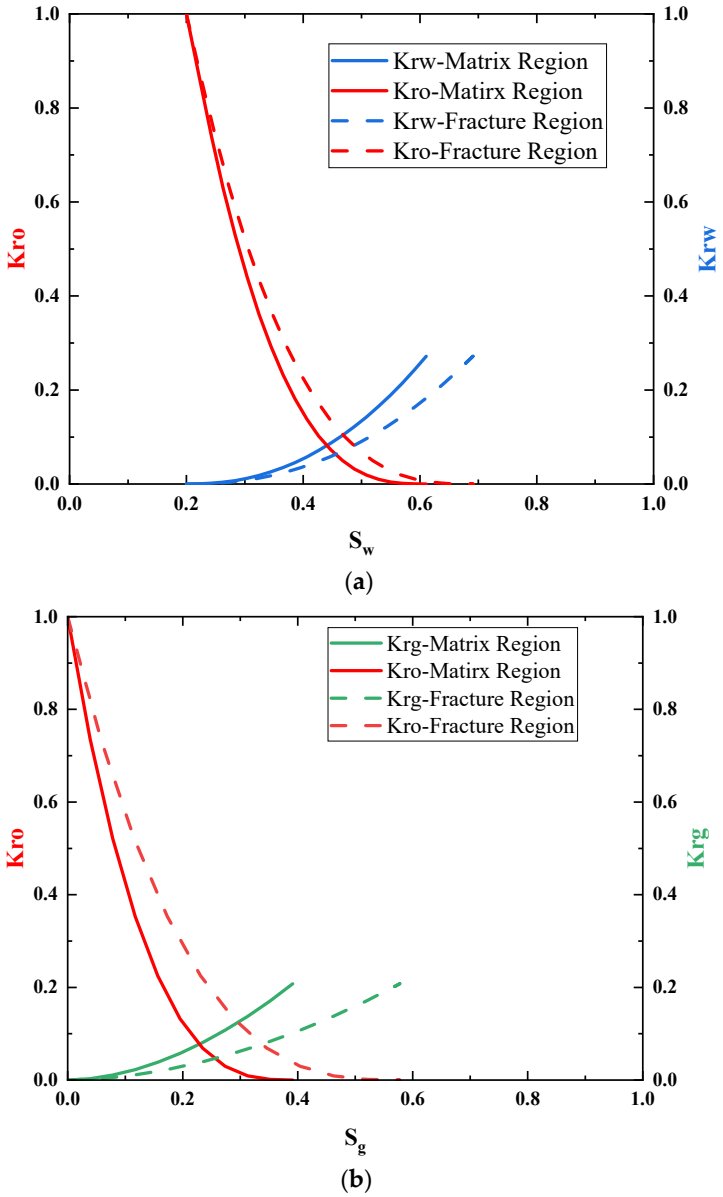


Figure 13. Relative permeability curves of the matrix and equivalent fracture zone: (**a**) oil–water phase relative permeability curve and (**b**) oil–gas phase relative permeability curve.

The model verification results are shown in Figure 14. As illustrated, the daily oil, gas, and water production rates calculated using the semi-analytical method proposed in this study were in close agreement with the results obtained from numerical simulation soft-

ware. The maximum error in oil, gas, and water production between the two methods was within 7%, demonstrating that the semi-analytical model met the engineering accuracy requirements. These results confirmed the reliability and high accuracy of the semi-analytical model developed in this paper, making it a robust tool for predicting multiphase flow dynamics in fractured reservoirs.

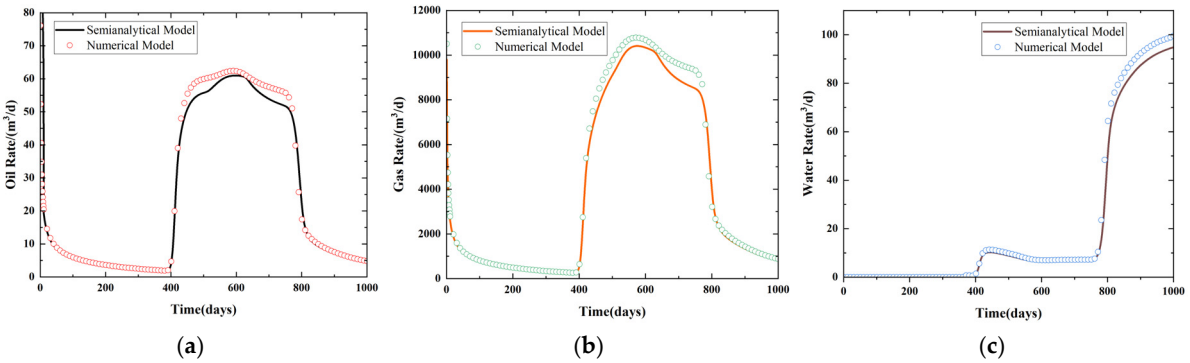


Figure 14. Semi-analytical model verification results: (**a**) comparison of oil rate, (**b**) comparison of gas rate, and (**c**) comparison of water rate.

3.3. Analysis of Factors Affecting Productivity of the Semi-Analytical Model

The productivity of a weakly volatile fractured reservoir is closely related to its geological characteristics, fluid parameters, and injection scenarios. Therefore, this paper used the semi-analytical model to analyze the influencing factors.

3.3.1. The Influence of Fracture Occurrence

The study analyzed different fracture distribution models, representing fracture-controlled areas as hyperpermeability zones, and simulated production and water injection scenarios. Results in Figures 15 and 16 showed that fully and partially penetrating fractures achieved higher oil and gas production than non-penetrating fractures, with larger fracture distributions leading to longer stable production periods and higher ultimate recovery. However, water injection in partially penetrating fractures resulted in earlier water breakthrough due to preferential flow along hyperpermeability channels [32,33]. These findings underscore the importance of fracture characterization for optimizing water injection strategies and enhancing recovery efficiency in fractured reservoirs, while managing the challenges of early water breakthrough.

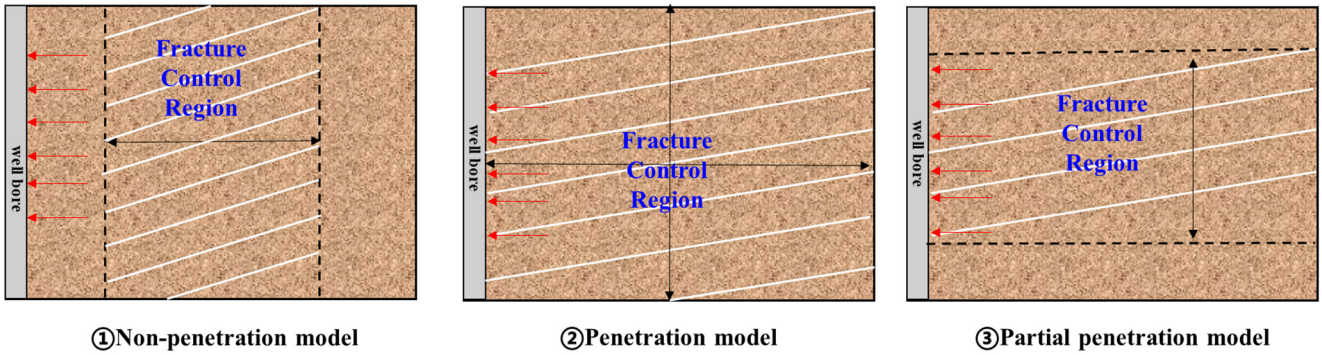


Figure 15. Fracture distribution characteristic model.

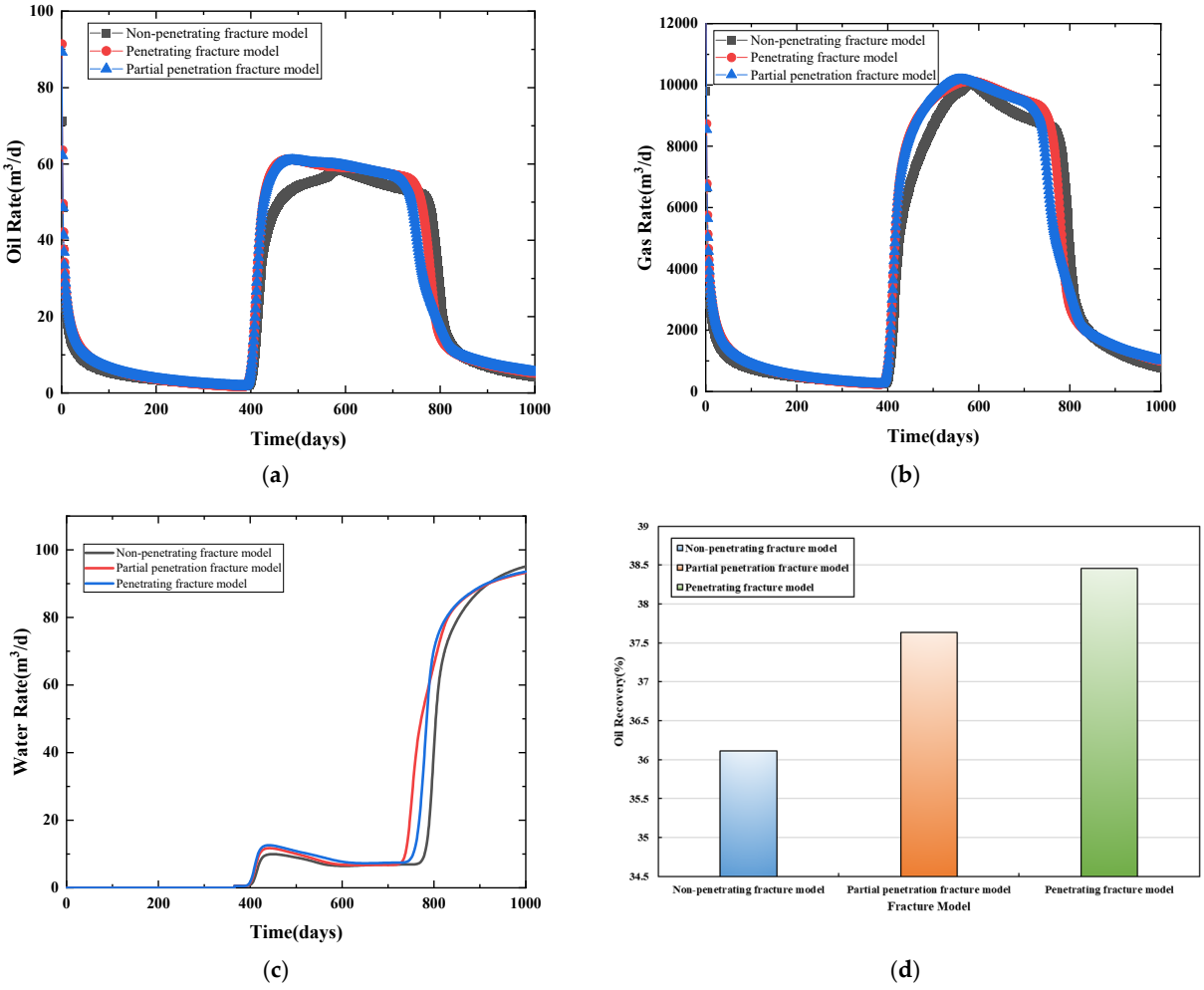
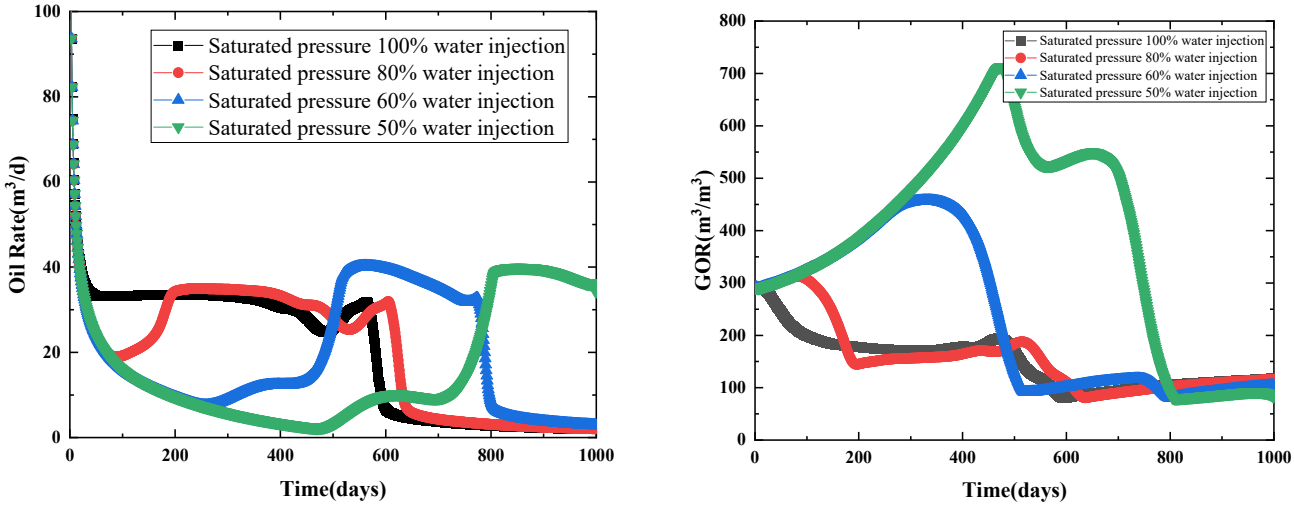


Figure 16. Calculation results of distribution models of different fracture occurrences: (**a**) comparison of oil rate, (**b**) comparison of gas rate, (**c**) comparison of water rate, and (**d**) comparison of oil recovery.

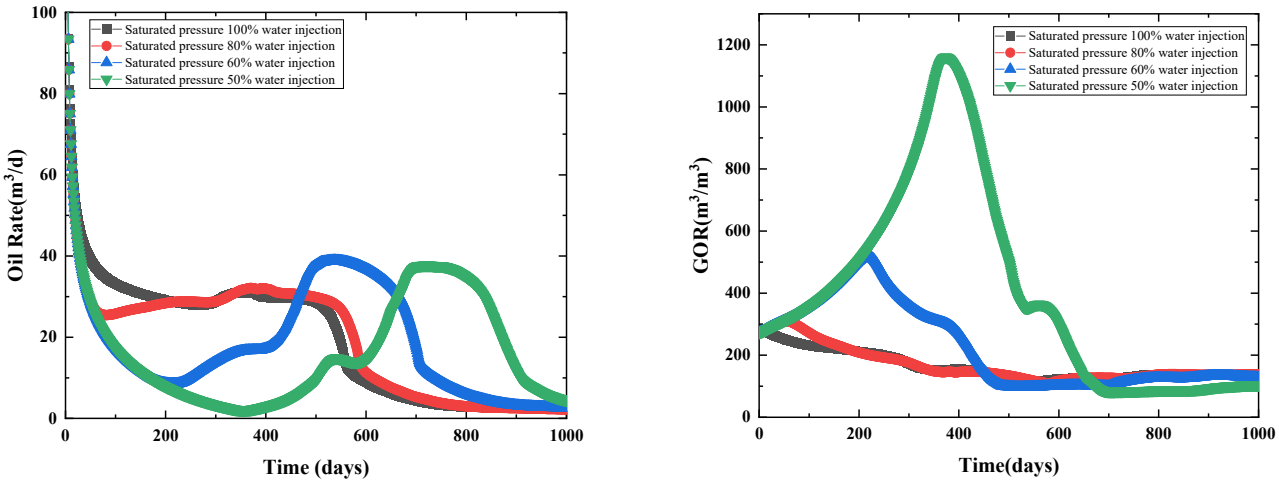
3.3.2. The Influence of Water Injection Timing

The study analyzed the impact of different water injection timings on productivity by selecting full-penetration and non-penetration fracture models. Water injection was performed when the reservoir pressure reduced to the bubble point pressure, 80% of the bubble point pressure, 60% of the bubble point pressure, and 50% of the bubble point pressure. As shown in Figures 17–19, earlier water injection more effectively recovered formation energy, prolonged stable oil and gas production, and resulted in higher cumulative oil production. Delayed water injection led to lower reservoir pressure drops, higher gas–oil ratios during production, and reduced oil and gas output in later stages. For non-penetrating fractures, the highest cumulative oil production was achieved when injection occurred at 80% of the bubble point pressure. In penetrating fractures, earlier water breakthrough necessitated earlier injection timing. For field applications, it is recommended to initiate water injection when the formation pressure drops to 80% of the bubble point pressure to balance cost efficiency and maximize recovery.



(**a**) (**b**)

Figure 17. Production history of different injection timings in the non-penetrating fracture model: (**a**) comparison of oil rate and (**b**) comparison of GOR.



(**a**) (**b**)

Figure 18. Production history of different water injection timings in the perforating fracture model: (**a**) comparison of oil rate and (**b**) comparison of GOR.

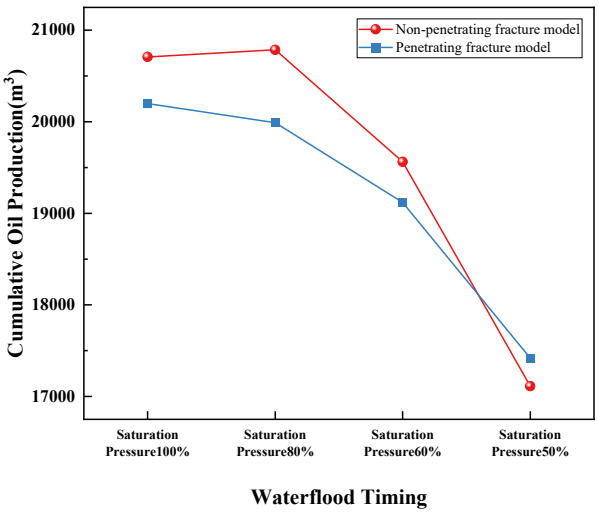


Figure 19. The cumulative oil production of different fracture models at different injection times.

3.3.3. Influence of Injection Method

To optimize injection strategies, full-penetration and non-penetration fracture models were analyzed, simulating three methods—continuous injection and continuous production, periodic injection and continuous production, and periodic injection and periodic production—when the average model pressure decreased to 80% of the bubble point pressure [34,35]. As shown in Figures 20 and 21, periodic-injection–continuous-production and periodic-injection–periodic-production methods achieved higher final recovery rates compared to conventional water flooding. Before water breakthrough, recovery efficiency differences between methods were minimal, but significant differences emerged after water breakthrough. In non-penetrating fracture models, water breakthrough times were similar across injection methods, whereas penetrating fracture models exhibited larger variations in breakthrough times, which significantly influenced the final recovery efficiency. These findings highlight the importance of injection timing and method selection for maximizing recovery in fractured reservoirs.

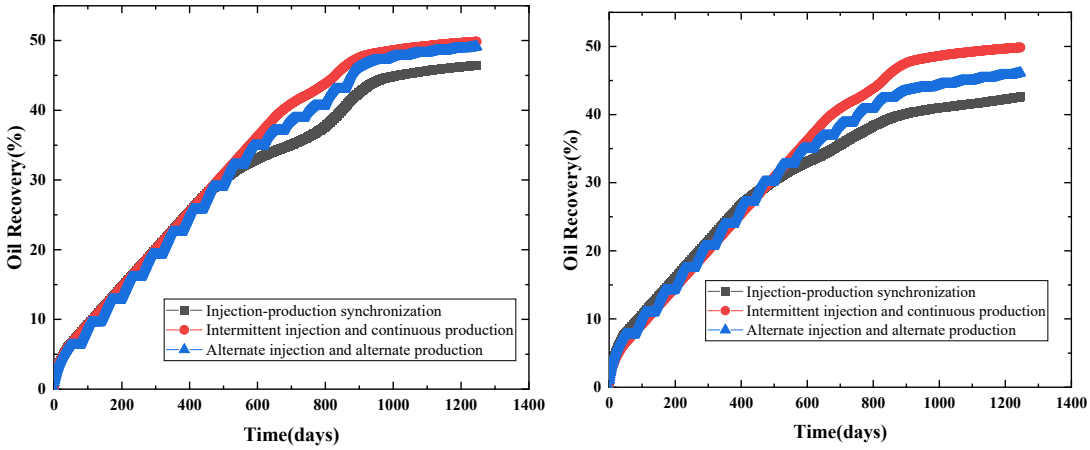


Figure 20. Comparison of recovery efficiency of different fracture models and injection methods. (**a**) Recovery efficiency of different water-flooding modes using the non-penetrating fracture model. (**b**) Recovery efficiency of different water-flooding modes using the fracture model.

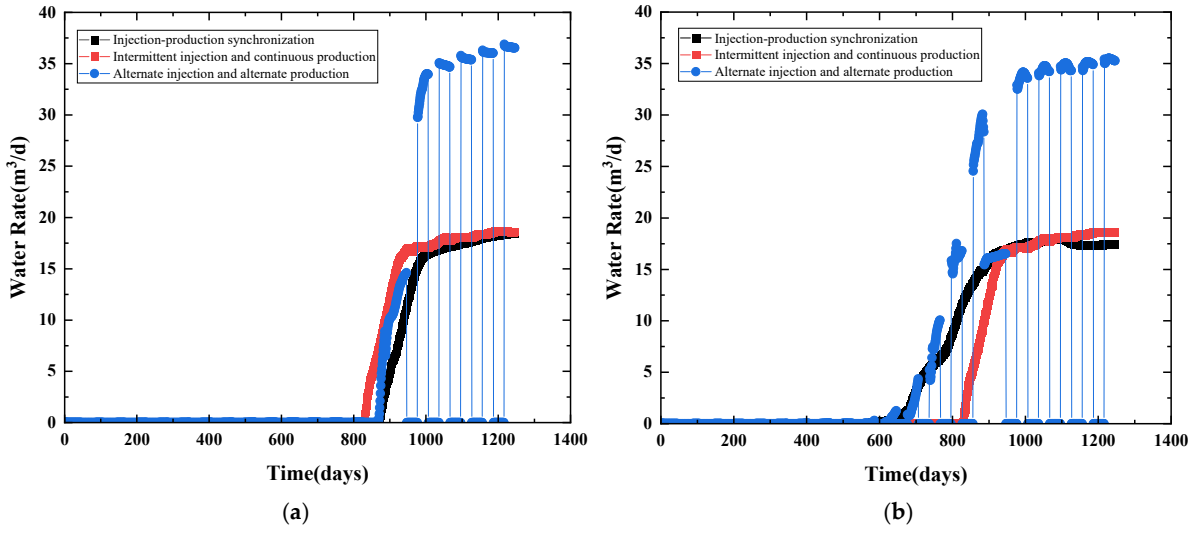


Figure 21. Comparison of the water rate in different fracture models and injection methods. (**a**) Water rate of different injection methods using the non-penetrating fracture model. (**b**) Water rate of different injection methods using the fracture model.

3.3.4. The Influence of Water Injection Duration

The through-fracture and non-through-fracture models were analyzed to optimize the water injection duration, ensuring consistent water injection intensity, production time, and total injection volume [36–38]. Average pressure, recovery efficiency, and daily water production were compared under varying injection durations. Results from Figures 22 and 23 indicated that the water injection duration had a greater impact on the through-fracture model than the non-penetrating fracture model. For the non-penetrating fracture model, water breakthrough timing remained consistent across different injection durations, with longer injection durations resulting in relatively higher recovery rates. In the through-fracture model, a 60-day water-flooding half-cycle achieved the latest water breakthrough and a higher recovery rate compared to 30-day and 50-day cycles. The operational parameters are listed in Table 3. These findings underscore the importance of optimizing the water injection duration to maximize recovery in fracture-developed areas.

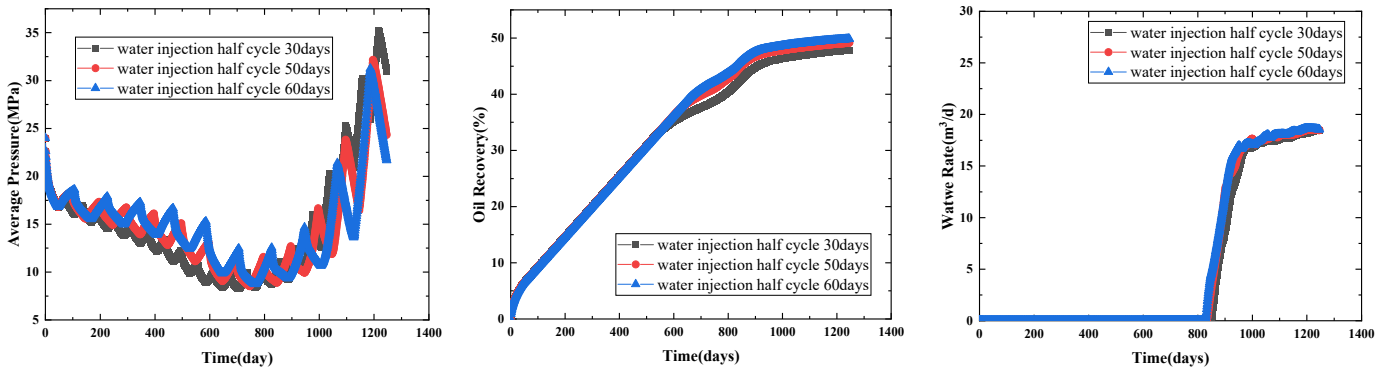


Figure 22. Results of different water injection durations using the non-penetrating fracture model: (**a**) average pressure, (**b**) oil recovery, and (**c**) water rate.

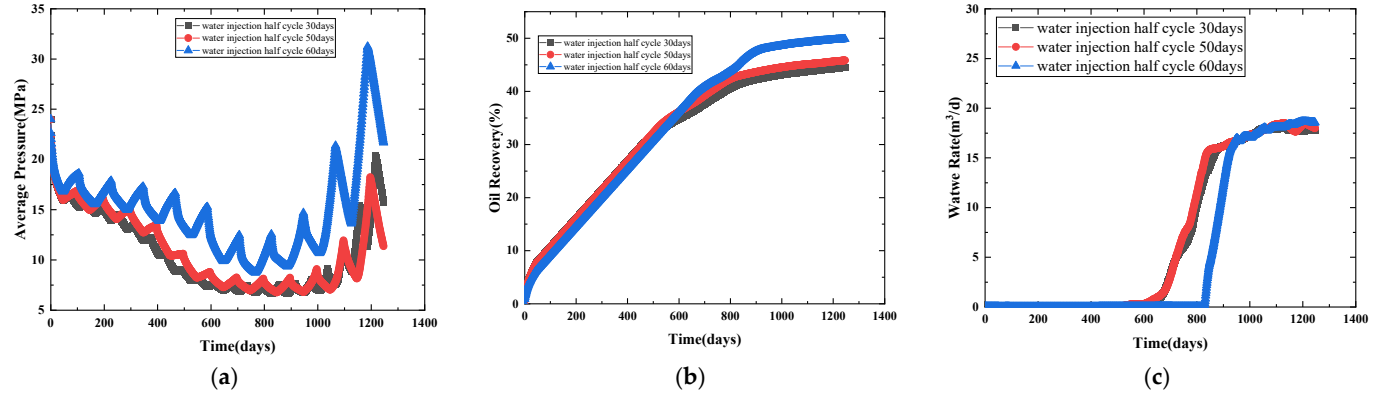


Figure 23. Results of different half-cycle water injections using the fracture model: (**a**) average pressure, (**b**) oil recovery, and (**c**) water rate.

Table 3. Design of different water injection durations.

Number of Cycles	Water Injection Duration	Water Injection Rate	Total Injection Volume
20	30 days	30 m^3/d	18,000 m^3
12	50 days	30 m^3/d	18,000 m^3
10	60 days	30 m^3/d	18,000 m^3

4. Conclusions

In this study, an equivalent fracture unit concept was proposed, and a method for calculating equivalent permeability was developed based on an analysis of core fracture occurrences in the field. A mathematical model for three-phase oil–gas seepage in water-flooded reservoirs, accounting for connate water saturation, was constructed. Furthermore, a semi-analytical productivity prediction method was established by combining the flow material balance principle with the dynamic drainage distance, enabling rapid prediction of oil–gas productivity in weakly volatile fractured reservoirs under water flooding. The main conclusions were as follows:

(1) Based on the analysis of field-fractured cores, the equivalent fracture unit concept was introduced, and a calculation method for equivalent permeability suitable for both individual fractures and fracture zones was developed. This provided a robust approach for modeling fractured zones.
(2) A three-zone, three-phase water-flooding mathematical model was constructed using the principle of material balance. By employing Newton iteration to solve for pressure and saturation at each time step and updating the nonlinear parameters, the model accurately addressed three-phase nonlinear oil–gas seepage, ensuring efficient and precise solutions.
(3) Numerical simulation results demonstrated that the proposed method achieved high accuracy, forming a multiphase zonal hybrid solution approach that satisfied the engineering requirements. This enabled rapid prediction of the production performance under varying geological characteristics and injection scenarios.
(4) Regarding the geological characteristics, the through-fracture model exhibited higher production rates, a wider fracture distribution, and a higher water-flooding recovery rate compared to the non-penetrating fracture model.
(5) For injection strategies, the optimal timing for water injection was when the formation pressure decreased to approximately 80% of the bubble point pressure. In the through-fracture model, water breakthrough occurred earlier than in the non-through-fracture model. Compared to conventional water flooding, periodic-injection–continuous-production and periodic-injection–periodic-production strategies improved oil and gas recovery efficiency, with the optimal water-flooding duration being 60 days.

Author Contributions: Conceptualization, W.Z., L.Z. and P.J.; methodology, W.Z., Q.W. and P.J.; software W.Z., L.Z. and P.J.; validation, W.Z., Q.W., Q.H. and J.H.; investigation, W.Z., Q.W., Q.H. and J.H.; writing—original draft preparation, W.Z.; writing—review and editing, Q.W., Q.H. and J.H.; supervision, L.Z.; project administration, L.Z.; funding acquisition, P.J. All authors have read and agreed to the published version of the manuscript.

Funding: This research was funded by PetroChina. The APC was funded by PetroChina.

Data Availability Statement: Data will be made available upon reasonable request.

Acknowledgments: The technical assistance provided by the China University of Petroleum (Beijing) is gratefully acknowledged by the authors.

Conflicts of Interest: Authors Wenqi Zhao, Lun Zhao, Qianhui Wu, Qingying Hou and Jue Hou were employed by the company PetroChina Research Institute of Petroleum Exploration & Development, China National Petroleum Corporation. The remaining authors declare that the research was conducted in the absence of any commercial or financial relationships that could be construed as a potential conflict of interest. The funders had no role in the design of the study; in the collection, analyses, or interpretation of data; in the writing of the manuscript, or in the decision to publish the results.

References

1. Marque, N.L.; Nogueira, C.G.; Cleto, P.R.; Maedo, M.A.; Rodrigues, E.A.; Manzoli, O.L. Parametric sensitivity analysis to select the relevant natural fractures in reservoir rock cells based on the equivalent permeability response. *Geoenergy Sci. Eng.* **2023**, *229*, 212051. [CrossRef]
2. Wei, L.; Zhechao, W.; Li, Q. Determination of REV size and equivalent permeability coefficient of fractured rock masses from the perspective of fracture network connectivity. *Comput. Geotech.* **2024**, *173*, 106590. [CrossRef]
3. Pakdel, P.; Pietruszczak, S. On quantification of equivalent permeability tensor in sparsely fractured rock masses. *Int. J. Rock Mech. Min. Sci.* **2024**, *178*, 105735. [CrossRef]
4. Fan, Z.; Guo, C.; Liu, W.; Yang, Z. Effect of fracture geometry on effective electrical properties of shale model using electrical tensor matrix. *Prog. Geophys.* **2021**, *36*, 2168–2177.
5. Zheng, J.; Xu, Q.; Zhang, B.; Guo, J.; Lü, Q.; Tan, S. A complex-network-based estimation of the representative elementary volume and equivalent permeability coefficient for fractured rock masses. *J. Hydrol.* **2024**, *638*, 131513. [CrossRef]
6. Gao, L.; Yang, J.; Li, J.; Bao, X. Building an equivalent fracture model and performing forward. *Geophys. Prospect. Pet.* **2020**, *59*, 404–408.
7. Zhang, S.; Ya, N.; Sun, H. An efficient calculation of equivalent permeability of fractured porous media based on discrete fracture model. *Sci. Technol. Eng.* **2014**, *14*, 36–40.
8. Snow, D.T. Anisotropie permeability of fractured media. *Water Resour. Res.* **1969**, *5*, 1273–1289. [CrossRef]
9. Long, J.; Witherspoon, P.A. The relationship of the degree of interconnection to permeability in fracture networks. *J. Geophys. Res. Solid Earth 1978–2012* **1985**, *90*, 3087–3098. [CrossRef]
10. Sagar, B.; Runchal, A. Permeability of fractured rock: Effect of fracture size and data uncertainties. *Water Resour. Res.* **1982**, *18*, 266–274. [CrossRef]
11. Liu, K. *Productivity Prediction of Fractured Reservoir*; China University of Petroleum (East China): Qingdao, China, 2017.
12. Ji, J.; Yao, Y.; Huang, S.; Ma, X.; Zhang, S.; Zhang, F. Analytical model for production performance analysis of multi-fractured horizontal well in tight oil reservoirs. *J. Pet. Sci. Eng.* **2017**, *158*, 380–397. [CrossRef]
13. Sureshjani, M.H.; Gerami, S. An analytical model for production data analysis of under saturated oil reservoirs subjected to edge aquifer. *J. Pet. Sci. Eng.* **2011**, *78*, 23–31. [CrossRef]
14. Wang, Y. *Research on the Law of Pressure Decline After Pressure in Fractured Reservoir*; Southwest Petroleum University: Chengdu, China, 2017.
15. Chen, X.; Liu, P. A semi-analytical solution under a variable inner boundary condition for fractured horizontal wells in a rectangular closed reservoir with discrete fracture networks. *Geoenergy Sci. Eng.* **2023**, *223*, 211529. [CrossRef]
16. Wang, Z.; Zhao, X.; Ong, S.; He, Y. Semi-analytical model-based research on influencing factors of the spacing of volume fracturing horizontal well in tight oil reservoirs via consideration of imbibition. *J. Pet. Sci. Eng.* **2021**, *198*, 108167. [CrossRef]
17. Yun, Z.; Zhijiang, K.; Junwei, M.A.; Huan, Z.; Dawei, W. A numerical simulation method for deep, discrete fractured reservoirs using a multi-scale fluid-rock coupling model. *Earth Sci. Front.* **2023**, *30*, 365–370.
18. Bai, Y.; Hou, J.; Clarke, M.A.; Zhao, E.; Zhang, B.; Liu, Y. Numerical Simulation on Reservoir Stimulation Assisted Depressurization Development of Hydrate Bearing Layers Based on Embedded Discrete Fractures. *Geoenergy Sci. Eng.* **2024**, *241*, 213112. [CrossRef]
19. Zhang, Z.; Xu, T.; Li, S.; He, J.; Li, X.; Li, Y.; Qin, X. Optimizing fracturing techniques for enhanced hydrate dissociation in low-permeability reservoirs: Insights from numerical simulation. *Gas Sci. Eng.* **2024**, *125*, 205309. [CrossRef]
20. Luo, M.; Jia, G.; Yang, Y.; Si, X.; Ge, Y.; Zhan, Y.; Lu, M. Numerical simulation of proppant transportation and placement in several complex structure fractures of a shale reservoir using a CFD approach. *Gas Sci. Eng.* **2023**, *118*, 205115. [CrossRef]
21. Qanbari, F.; Clarkson, C.R. Rate-Transient Analysis of Liquid-Rich Tight/Shale Reservoirs Using the Dynamic Drainage Area Concept: Examples from North American Reservoirs. *J. Nat. Gas Sci. Eng.* **2016**, *35*, 224–236. [CrossRef]
22. Shenglai, Y.; Junzhi, W. *Reservoir Physics*; Petroleum Industry Press: Baijing, China, 2004.
23. Feng, J.; Cheng, L.; Li, C.; Liu, L. Equivalent continuum model of fractured low permeability reservoir. *Pet. Drill. Tech.* **2007**, *35*, 94–97.
24. Clarkson, C.R.; Qanbari, F.; Behmanesh, H. An Approximate Analytical Multi-Phase Forecasting Method for Multi-Fractured Light Tight Oil Wells with Complex Fracture Geometry. In Proceedings of the Unconventional Resources Technology Conference, San Antonio, TX, USA, 20–22 July 2015. [CrossRef]
25. Wang, Z.; Cheng, L.; Hamdi, H. A semi-analytical model for quantifying the inter-well communication in water-bearing shale gas-condensate reservoirs. *Geoenergy Sci. Eng.* **2023**, *228*, 211997. [CrossRef]
26. Wattenbarger, R.A.; El-Banbi, A.H.; Villegas, M.E.; Maggard, J.B. Society of Petroleum Engineers SPE Rocky Mountain Regional/Low-Permeability Reservoirs Symposium—Denver, Colorado (1998-04-05) SPE Rocky Mountain Regional/Low-Permeability Reservoirs Symposium—Production Analysis of Linear Flow into Fractured Tight G. In Proceedings of the SPE Rocky Mountain Regional/Low-Permeability Reservoirs Symposium, Denver, CO, USA, 5–8 April 1998. [CrossRef]

27. Ding, L.; Wu, Q.; Zhang, L.; Guérillot, D. Application of fractional flow theory for analytical modeling of surfactant flooding, polymer flooding, and surfactant/polymer flooding for chemical enhanced oil recovery. *Water* **2020**, *12*, 2195. [CrossRef]
28. Wu, Q.; Ding, L.; Zhang, L.; Ge, J.; Rahman, M.A.; Economou, I.G.; Guérillot, D. Polymer enhanced foam for improving oil recovery in oil-wet carbonate reservoirs: A proof of concept and insights into the polymer-surfactant interactions. *Energy* **2023**, *264*, 126256. [CrossRef]
29. Wu, Q.; Ding, L.; Zhao, L.; Alhashboul, A.A.; Almajid, M.M.; Patil, P.; Zhao, W.; Fan, Z. CO_2 soluble surfactants for carbon storage in carbonate saline aquifers with achievable injectivity: Implications from the continuous CO_2 injection study. *Energy* **2024**, *290*, 130064. [CrossRef]
30. Wu, Q.; Ding, L.; Zhao, L.; Zhao, W.; AlYousef, Z.; Alsaud, M.A.; Fan, Z. Dynamic adsorption of switchable amine surfactants on carbonate under reservoir conditions: Implications for foam assisted CO_2 storage. *Chem. Eng. J.* **2024**, *496*, 154003. [CrossRef]
31. Baker, L.E. Three-Phase Relative Permeability Correlations. In Proceedings of the SPE Enhanced Oil Recovery Symposium, Tulsa, Oklahoma, 16–21 April 1988.
32. Wu, Q.; Ge, J.; Ding, L.; Wei, K.; Deng, X.; Liu, Y. Identification and characterization of a proper gel system for large-volume conformance control treatments in a fractured tight reservoir: From lab to field. *J. Pet. Sci. Eng.* **2021**, *198*, 108199. [CrossRef]
33. Wu, Q.; Ge, J.; Ding, L.; Wei, K.; Liu, Y.; Deng, X.B. December. A successful field application of polymer gel for water shutoff in a fractured tight sandstone reservoir. In *SPE Middle East Oil and Gas Show and Conference*; SPE: Richardson, TX, USA, 2021; p. D031S028R008.
34. Patel, S.M.; Sondergeld, C.H.; Rai, C.S. Laboratory studies of hydraulic fracturing by cyclic injection. *Int. J. Rock Mech. Min. Sci.* **2017**, *95*, 8–15. [CrossRef]
35. Liu, Y.; Xu, T.; Yuan, Y.; Feng, B.; Tang, X.; Liu, X.; Cui, Z. A laboratory study on fracture initiation and propagation of granite under cyclic-injection hydraulic fracturing. *J. Pet. Sci. Eng.* **2022**, *212*, 110278. [CrossRef]
36. de Swaan, A. Theory of waterflooding in fractured reservoirs. *Soc. Pet. Eng. J.* **1978**, *18*, 117–122. [CrossRef]
37. Belayneh, M.; Geiger, S.; Matthai, S.K. Numerical simulation of water injection into layered fractured carbonate reservoir analogs. *AAPG Bull.* **2006**, *90*, 1473–1493. [CrossRef]
38. Wang, Y.; Cheng, S.; Feng, N.; Xu, J.; Qin, J.; He, Y.; Yu, H. Semi-analytical modeling for water injection well in tight reservoir considering the variation of waterflood-Induced fracture properties–Case studies in Changqing Oilfield, China. *J. Pet. Sci. Eng.* **2017**, *159*, 740–753. [CrossRef]

Disclaimer/Publisher's Note: The statements, opinions and data contained in all publications are solely those of the individual author(s) and contributor(s) and not of MDPI and/or the editor(s). MDPI and/or the editor(s) disclaim responsibility for any injury to people or property resulting from any ideas, methods, instructions or products referred to in the content.